

Period and length of high surface gravity waves measured in the coastal waters of eastern Arabian Sea and its variations in 10 years

Anju T M¹, Sanil Kumar V¹, Jai Singh¹, Bhaware B.G²

¹Ocean Engineering Division, CSIR-National Institute of Oceanography
(Council of Scientific & Industrial Research), Dona Paula 403 004, Goa, India

²Department of Zoology, G. M. Vedak College of Science,
Tala–Raigad 402111 Maharashtra, India
Correspondance to email: sanil@nio.org

Abstract

Information on the period and length of waves is required for the planning and design of marine facilities and wave energy converters. In this article, the period and length of the waves measured during the peak monsoon (June-July) in the coastal waters of the eastern Arabian Sea for 10 years are examined. The most typical wave periods (T) are within 3.9 s and 5.5 s and about 25% are above 9 s. The peak wave period (T_p) indicates that during the peak monsoon months, long-period waves dominate the eastern Arabian Sea. Significant wave period and integral wave period show a good linear relationship with energy wave period with a slope value close to 1. There are inter-annual variations of up to 15% in the 90-percentile value of the T_p . From 2010 to 2019, the average wavelength during peak monsoon varied from 61.3 m to 67.6 m and the maximum wavelength from 216.6 m to 248.8 m. Interannual variations in the 90-percentile values for wavelength corresponding to maximum wave height is only 7%.

Key Words: wind waves, wavelength, wave spectral parameters, Indian summer monsoon, Ocean sciences

1.Introduction

The wave load generally increases with the wave height but also depends significantly on the wave period. In the ocean, waves come from different sources: sea waves (periods between 2 and 7 s) generated by local winds; swell waves (periods 7 to 25 s) generated by storm systems far away; infra gravity waves (periods 25 to 120 s) resulting from the swell interacting with the coastline; and far infra gravity waves (periods 120 to 360 s) resulting from groups of swell waves. These waves form a spectrum that may be a single peak or could have many peaks, one for each wave type. The high waves present during calm local weather are entirely from swell waves that have been generated thousands of kilometres away, giving mean wave periods of 15 s or more. The upper limit of the period measured by the buoys depends on its lower frequency limit. For simulated waves from a model, the lower frequency limit in the model is set arbitrarily by the modeller.

In most of the studies, the mean apparent wave period (T_{m02}) is used as mean wave period, and T_{m02} is the most widely used parameter to describe a sea state (WMO, 1998). The value of the T_{m02} describes the type of wave that is dominant in a particular area. T_{m02} is sensitive to the high-frequency cut-off. For buoy data, the cut-off frequency is at 0.5 to 1 Hz and for the model, the cut-off is generally at 0.5 Hz. Mean values of T_{m02} change by 10% if the upper-frequency limit is decreased from 1.0 Hz to 0.4 Hz. The earlier studies have shown that T_{m02} gives the closest result to the period obtained from the zero-crossing method. The significant wave period ($T_{1/3}$) estimated from the zero-crossing analysis is used in the design of coastal structures (Goda, 2010). Several researchers tried to find the correlation between $T_{1/3}$ and the wave period obtained from the wave spectrum.

Offshore facilities face more hostile natural conditions than ports, especially the long-period waves. Long-period waves have considerable energy that can easily cause a large amplitude motion of moored ship (Shen et al., 2016). Cyclic loading fatigue of structures depends on the wave period. In most of the studies, T_{m02} is used. In some studies, mean period (T_{m01}) resulted from the ratio between m_0 and m_1 is used. T_{m01} is defined as the period computed from the first frequency moment of the wave spectrum. The period of the spectral peak (T_p) dictates the celerity of the dominant waves, and is therefore critical to the forecasting of the time of arrival of waves at the coast. T_p also provides an indication of the source of waves, i.e., locally generated or distally generated. The T_p represents unimodal spectra and representing a complicated sea state by a single parametric variable can mask the true nature of the observed sea state. When there is a mixture of wind-sea and swell, T_p can be noisy (Young, 1999). A bimodal distribution of wave periods causes significant coastal damage and beach morphology changes (Bradbury et al., 2007).

Wave energy period (T_e), i.e., the wave period of a simple sinusoidal wave that would carry the total energy of the waves happening during a fixed time frame (30 minutes) is the one which is used to characterize wave energy. Often the power matrices of the wave energy converters are provided using the T_p , or T_{m02} , or T_{m01} along with significant wave height (H_s). The period T_e gives more weight to the longer wave periods in a spectrum and is suitable for multi-peaked spectra (Van der Meer et al., 2016) and T_e is the characteristic wave period when describing the hydraulic attack on coastal structures. T_e is provided as the mean wave period in the WAM model (Günther et al., 1992). T_{m02} is less noisy than the usual T_p and attaches great importance to the low-frequency part of the spectrum (Rawat et al., 2014). T_{m01} is used in many studies instead of T_p because T_p is a noisier parameter and T_{m01} is a weighted average, which considers the distribution of energy across frequencies.

It is important to highlight the fact that the wave periods obtained from these methodologies are different and should be selected depending on the user application. Also, it is important to know how these wave periods compare to each other. For the planning and design of marine infrastructure and wave energy converters, knowledge of wave period and wavelength is essential. Understanding wave duration is crucial in marine engineering for constructing structures that can withstand wave forces. When opposed to shorter, more frequent waves, longer wave durations place less dynamic loading on structures, which has an effect on the construction of offshore platforms, piers, docks, and breakwaters. Information on wave period and length is used to control mooring systems for ships and offshore construction. For stability and safety, these systems must be designed to handle particular wave characteristics. The efficiency of wave energy converters (WECs) depends on the wave period. WECs work best when their oscillations match the frequency of the incident waves.

The wavelength at a location and the length of the structure are required to carry out hydro-elastic analysis of a very large floating structure (Suzuki et al., 1996). The wave drift force which is proportional to the square of the wave height must be considered when the length of a floating structure becomes equal or larger than the wavelength (Ueda et al., 2015). Hence, it is important to know the various wavelength statistics at a location.

The waves in the coastal waters of the eastern Arabian Sea (AS) are high during June and July due to the strong winds generated by the Asian summer monsoon (Anoop et al., 2015). Several factors can influence the wave characteristics in the coastal waters of the eastern Arabian Sea. Variations in wind patterns can influence the monsoon and the local winds, which creates a significant impact on wave behaviour. The maximum wave height from 2010 to 2018 in the eastern AS occurred either in June or July (Anjali Nair et al., 2022) and the individual wave period, height,

length and steepness are higher during the monsoon (Anusree and Kumar, 2023). In the eastern AS, the depression formed during the summer monsoon resulted in the highest wave heights along this coast even though they are short-lived lasting a few days (Kumar et al., 2020). Along the west coast of India, wave climate dominates wind-seas and swells (Kumar et al., 2014). Earlier studies also indicate that waves during the summer monsoon period are higher than those due to the tropical cyclones formed during the non-monsoon period (Kumar et al., 2020). The variations in significant wave height and mean period of monsoon waves in the eastern AS are studied by many researchers (Anand et al., 1994; Rao and Baba, 1996; Amrutha and Kumar, 2017; Kumar et al., 2000; Kumar et al., 2020; Anju and Kumar, 2023). The earlier studies indicate that there are significant inter-annual variations in wave characteristics due to the variations in summer monsoon (Kumar and George, 2016). The waves in the Indian Ocean are also influenced by various atmospheric oscillations such as El Niño Southern Oscillation (ENSO) (Hemer et al., 2010; George and Kumar, 2021; Liu et al., 2023), Southern Annular Mode (SAM) (Liu et al., 2022), Indian Ocean Dipole (IOD) (Anoop et al., 2016; Kumar et al., 2019; Liu et al., 2023) and Boreal Summer Intra-Seasonal Oscillation (BSISO) (Joseph and Kumar, 2021). Hence, it is important to examine the inter-annual variations of the wave period of high waves.

Against this background, the present study aims to shed light on the characteristics of the period and length of high waves measured in the eastern Arabian Sea and its interannual variations in 10 years. This study is based on the continuous measured wave buoy data from 2010 to 2019. For the first time, we discuss the probability distribution of all characteristic wave periods and associated wavelengths in the coastal waters of the eastern Arabian Sea that are required in different applications. The rest of the paper is structured as follows. Data and methods are described in Section 2. Section 3 deals with the results and discussions and Section 4 gives a summary and conclusion from the study.

2.Data and methods

The measured wave data using the moored 0.9 m diameter Datawell Directional Waverider Mk III buoy (Datawell, 2009) from 1 June to 31 July for 10 years from 2010 to 2019 is used in the study and there was no data gap for the period selected. The location of the buoy is 2 km offshore and the water depth at the measurement site is 13 m (Fig. 1). The buoy is moored using an anchor chain with a weight of about 400 kg, a 15 m long 35 mm diameter rubber cord and a 20 m long 16 mm diameter polypropylene rope. The vertical and horizontal accelerations (which are then integrated twice) of the buoy during a 30-minute time span, at a frequency of 3.84 Hz are sampled and logged at a sampling frequency of 1.28 Hz. Data recorded for 30 minutes are saved as one record

and are used for different analyses. Heave is measured with 3% accuracy and 1 cm resolution (Datawell, 2009). The variation in water depth due to tide is neglected in the present study. The height (H) and period (T) of the individual wave are obtained from the zero up-crossing method (Tucker, 1991). The maximum height in a 30-minutes duration is maximum wave height (H_{max}) and the period of this wave is T_{Hmax} . The average period of 10% and 33% highest waves in the 30-minutes record, i.e., $T_{1/10}$ and $T_{1/3}$ are also used in the analysis. Crest period (T_c) is obtained by dividing the length of the record by the number of crests in the record. T_{avg} is the ratio of the length of the record with the number of zero-up-crossing in that record.

The wave spectrum of surface elevation is estimated from the measured heave data at every 30-minutes through a Fast Fourier Transform. The wave spectrum obtained is with a resolution of 0.005 Hz from 0.025 Hz to 0.1 Hz and after that, it is 0.01 Hz up to 0.58 Hz (Datawell, 2009). The integrated wave parameters derived from the spectra and used in the study are significant wave height (H_s), mean zero-crossing period (T_{m02}), integral wave period (T_i), wave period corresponding to the mean frequency of the spectrum (T_{m01}), energy wave period (T_e), T_{dw1} , average wave period obtained using spectral moments ($T_{m-1,1}$), calculated peak period (T_{pc}). The wave period corresponding to the peak of the spectrum (T_p) is noted. The definition of wave parameters used in the study is given in Annexure.

Wavelengths (λ) corresponding to various wave periods are estimated from the respective wave period and the water depth by iteratively solving the wave dispersion relation. The percent of occurrence is calculated with 0.5 s bin (0,0-0.5,0.5-1,...) for the wave period and 10 m bin (0,0-5,5-10,...) for its corresponding wavelength. The 99 percentiles for June-July are taken as an extreme value index and are computed for all the wave periods and wavelengths.

3.Result and discussions

3.1Distribution of wave period

The various wave periods estimated from half-hourly records from 2010 to 2019 are presented as date versus year plot in Figure 2 and their statistical parameters are presented in Table 1. Wave periods of individual waves have a wide range. Waves with periods of 3.9 s and 5.5 s are the most frequent. About 50% of all seas are within the period range of 4.7-9.0 s and about 25% is above 9 s. During the monsoon months of June and July, T_{m02} and T_{avg} show a similar pattern. Similar variation is also observed for the parameters $T_{1/3}$, T_e and T_i (Fig. 2g to 2i). Around 80% of the values for T_p are greater than 8 s (Fig. 2m). The variation in H_s across the years is not the same. According

to Glejin et al. (2015), at Ratnagiri, the inter-annual changes in the annual average peak period range from 0.1 to 0.5 s, and the inter-annual variation in the annual average H_s is ~ 0.1 m.

Figure 3a represent the percentage occurrence of various wave periods for the whole 10 years. The distribution of the occurrence of most wave periods has a general bell shape, except T_c and T_p . The maximum occurrence of T_p is about 23.68% which occurs at 11-11.5 s. Bromirski et al. (2005) classified waves into short-period waves ($T < 6$ s), long-period waves ($T > 8$ s), and intermediate-period waves ($6 \text{ s} \leq T \leq 8 \text{ s}$). The overall percentage of $T_p < 6$ s (short-period waves) is about 0.14% and the value for $T_p > 8$ s (long-period waves) is 98.45%. The percentage of values in between $6 \text{ s} \leq T_p \leq 8 \text{ s}$ (intermediate-period waves) is about 1.41%. According to the percentage values obtained, for all years analysed long-period waves dominate with 98.45% which indicates the dominance of long-period waves or swells during peak monsoon months. In comparison to other seasons, the southwest monsoon has a higher percentage of long-period waves (Kumar and Mandal, 2022). Depending on geographic location, prevailing weather patterns, and local coastline characteristics, long-period waves and short-period waves may or may not occur during the peak monsoon months. During the peak monsoon months, long-period waves may prevail, influencing coastal wave conditions and the possibility of erosion, while short-period waves produced by locally generated winds might generate turbulent conditions near the coastal regions.

The half-hourly mean values of various wave parameters over 10 years are calculated and presented in Figure 4 which shows the probability of exceedance of wave periods during the peak monsoon months from 2010 to 2019. The result indicates that among all the years analysed the wave periods during 2014 exceeded more than the other wave periods except in the case of T_p (Fig. 4j) and T_c (Fig. 4a). For all years in the present study, the peak period (T_p) ranges between 4 s and 20 s (Fig. 4j) and the maximum of 99-percentile value (18.2 s) is observed in 2016. Even though the southern part of the Arabian Sea is open to the south Indian Ocean and Southern Ocean, a large longitudinal fluctuation in T_p is seen throughout the year (George and Kumar, 2020). The value of the T_{m02} describes about the type of wave that is dominant in a particular area. The 75% and 25% values of T_{m02} fall below 7.1 s and 6.2 s. Kumar and George (2016), reported that higher values for T_{m02} , T_p and $H_{1/3}$ were observed in 2014 due to the Tropical Cyclone Nanauk that formed in central AS, and higher 99, 90 and 75 percentile values were also observed in 2014 at Honnavar, 350 km south of the present study area. Long-period waves that travel from West to East in the North Atlantic Ocean basin are linked to an increase in T_{m02} throughout the winter (Shen et al., 2016). Minimum to maximum values of T ranges from 1.6 to 21.6 s. The Integral period (T_i), based on the moment of order -2, has higher values of about 12.5 s for the year 2014 (Fig. 4f). T_{m01} based on the first moment

is the period corresponding to the mean frequency of the spectrum which is used to estimate the magnitude of Stokes drift (Stokes, 1880) transport in deep water. A minimum value of 4.8 s and a maximum value of 11.3 s is observed for the average wave period ($T_{m-1,1}$) calculated using spectral moments. The mean values for T_{avg} , $T_{1/10}$, T_{dw1} are 6.9, 9.3, and 9.8 s. At Ratnagiri, the percentage of T_{Hmax} less than 6 s is about 0.66. 100% of the values for T_c is less than 6 s. The average wave period (T_{avg}) (Fig. 4d) in 30-minutes record ranges from 4.0 to 10.7 s. Half of the records showed period shorter than 6.9 s. Mean values for the parameters T_{m01} , $T_{1/3}$ and T_{Hmax} are 7.4, 9.1 and 9.3 s. Around 25% values for T_{Hmax} and $T_{1/3}$ is less than 8.4 s. Mode values of T_c , T_p and T_{pc} are 3.8, 11.1 and 11.7 s. Several wave periods, including the peak period T_p and the major zero-crossing period $T_{1/3}$, are related to a variety of coastal processes for typical spectral shapes and deep-sea circumstances (Hofland et al., 2017). The energy wave period (T_e) has a significant role in offshore power calculations and the energy period can be calculated from other variables like the mean or peak period when the spectral form is unknown (Hofland et al., 2017). The values of T_e (Fig. 4e) vary from 5.5 to 12 s. About 23.5% of T_e (Fig. 3a) occurs between 7 s and 7.5 s and there is no occurrence for $T_e > 12$ s. T_e is used to characterize the wave energy, a mode value of 9.0 s is observed for T_e and the 75 percentile and 25 percentile values are up to 9.2 s and 8.1 s.

3.2 Interannual variations in wave period

The distribution of the period of individual waves during June-July in different years indicates that relatively higher period waves ($T > 12$ s) are more during 2014, whereas lower period waves ($T < 4$ s) are more during 2015. In comparison with other years, about 20% of the values of wave period (T) during 2015 are less than 4 s and during other years, the percentage of $T < 4$ s is less than 20%. An increase in long-period waves during 2014 is due to the occurrence of Tropical Cyclone Nanauk, which originated from a low-pressure area over the east-central Arabian Sea (IMD, 2014). Variations in different wave periods were generated by the combined effects of the summer monsoon and the cyclonic storm. The changes in monsoon intensity are the primary cause of the interannual variability. 29% of the waves are with periods less than 4 s, while 1.3% of the waves are with periods more than 12 s. The 99-percentile values of all wave periods show an increase in 2014 (Fig. 5). The crest periods are mostly concentrated in a narrow range of 2.4-5.8 s and their 99-percentile value has the lowest variation over the years.

The 90-percentile and the mean value of T_p (Fig. 5b) reached a maximum of 14.3 s and 11.6 s, respectively in 2014 and the mean value was lowest (10.7 s) in 2015 and 2011. Interannual variations in the 90-percentile value of T_p is up to 15% (Fig. 6b). The variation in 99-percentile of T_c is less than 4% (Fig. 6a) and this minimal variation of T_c over the years shows the stable

characteristics of wave crests and is important for stability considerations and structural design for offshore structures and marine installations. A maximum 99-percentile value of 12, 13.5, 12.1 and 9.6 s are observed for T_i , T_{Hmax} , $T_{1/3}$ and T_{avg} in 2014 compared to other years. The values of T_e vary between 5.5 s and 12 s with a minimum mean value of 8.5 s in 2011 and 2015. The 90-percentile value for T_e (9.1 s) is lower for 2011. The maximum mean value for T_{dwl} is 10.4 s. Interannual variations in the 99-percentile values for T_{m02} and T_{m01} are up to 10% and 11%.

The interannual variations in the average wave period (T_{avg}) are up to 4%. Overall, the interannual variations provide information for assessing potential risks associated with maritime activities, coastal infrastructure design, disaster preparedness, and climate change impacts on coastal regions.

3.3 Relationship between various wave periods

Inter comparison of T_e with various wave periods indicates that values of $T_{m-1,1}$, $T_{1/3}$ and T_i are close to the value of T_e (Figs. 7a, d, h). Goda (2010) reported that $T_{1/3}$ is similar to T_e . When T_e is not available, the wave power is calculated using T_p (Contestabile et al., 2015). For the study area, T_p values are much higher than T_e and hence computing wave power using T_p will result in overestimation of wave power. The parameters $T_{m-1,1}$, $T_{1/3}$ and T_i show less scatter in comparison with the other parameters. Variation of T_e with T_p , T_{dwl} and T_{Hmax} is presented in Figs. 7e to 7g, and the relationship of these parameters shows a wide scatter. The slope of $T_{1/3}$ (0.96) and T_i (0.95) is close to 1 indicating a strong linear relationship with T_e and implies that changes in the significant wave period and integral period have a relatively proportional effect on the energy wave period. The relationship between these parameters provides insights into the characteristics of ocean waves. When the wave spectrum is quite narrow, $T_{1/3}$ and T_e are close to each other and this is due to the fact that $T_{1/3}$ denotes the most significant wave period, which are the waves that also represent the highest energy. By integrating the wave energy spectrum across all frequencies, T_i is determined. Depending on the specific characteristics of the wave spectrum, the relationship between T_i (integral wave period), $T_{1/3}$ (significant wave period), and T_e (energy wave period) is determined. The relative values of these parameters can vary based on the shape and energy distribution of the wave spectrum. It is important to consider the spectral characteristics when interpreting these wave period parameters.

Chun and Suh (2018) also observed that T_e compares well with $T_{1/3}$ for waves in the East Sea of Japan. Even though there is a large scatter between the calculated peak period (T_{pc}) and T_p , overall, it compared well with the T_p (Fig. 7l). In comparison to the T_e estimates from the

JONSWAP spectrum ($T_e = 0.9T_p$), and the Pierson-Moskowitz spectrum ($T_e = 0.86T_p$), T_e estimates are lower ($T_e=0.786 T_p$) because the study area frequently consists of many wave systems. Also, a large scatter is observed between T_e and T_p (Fig. 7e). Hemer et al. (2017) reported that for the waves in the coastal waters of Australia, $T_e= 0.857 \times T_p$. For the waters around the US, T_e/T_p ratio is 0.79 to 0.85 with larger values for the waters in the Gulf of Mexico (Ahn, 2021). Hofland et al. (2017) considered a prediction formula for T_e and the result shows that for shallow foreshores, T_e increases as water depth decreases up to 8 times the offshore value and it is comparatively low for milder slopes. According to Mendes and Oliveira (2021), the mean value of T_{m02} at Faro, Nazare and Leixoes ranges between 6 s and 7 s with a minimum value of 3 s to a maximum of 15 s. At Versova, Ratnagiri, Vengurla and Karwar, the significant wave period ($T_{1/3}$) compares well with the average wave period ($T_{m-1,1}$) with a correlation coefficient of 0.88–0.94 (Kumar and Mandal, 2022). Chun and Ahn (2017) model shows that for a maximum value of H_s of about 5.35 m, the predicted and measured values for $T_{1/3}$ are 9.79 s and 9.58 s at Hamada during a storm period. The eastern AS annual mean T_p is about 10.1 s indicating AS as a swell-dominated zone, the values of T_p varied from 2.3 s to 22.1 s, with a spatial variation in T_p up to 12% (George and Kumar, 2020). The monthly average value of the mean wave period is about 6.5 s to 7.5 s in Bay of Bengal (BoB) from 2013 to 2015 and the annual variation in the mean wave period is low when compared with the peak wave period in BoB (Anjali et al., 2018). Anjali et al. (2018) mentioned that during the pre-monsoon months in the BoB, the mean wave period decreases and gradually increases during the southwest monsoon, reaching maximum value in October and then decreasing. For a peak enhancement mean value of 3.3 in a JONSWAP spectrum, $T_e = 0.538 T_m$. For the present study area, $T_e = 1.158 T_{m01}$ (Fig. 7c). The relationships between various wave periods proposed in this study can be used for evaluation of the wave power of different WECs since the power matrix of these WECs is specified in terms of different wave periods.

H_s found to have a better correlation with T_{m02} than T_p (Figs. 7i and 7k). The large scatter in H_s compared to T_p is due to the presence of low amplitude ($H_s \sim 1-2$ m) long-period waves (14-20 s) in the study area. The mean value of the ratio between the maximum wave height in a 30-minutes record (H_{max}) and the corresponding H_s is 1.65 (Fig. 7j). In the present study, the H_s values range between 0.6 m and 5 m. Kumar et al. (2019) observed that, during El Nino years in the Arabian Sea, H_s is relatively low. According to George and Kumar (2020), along the west coast of India, the mean wave period is 10–25% greater during the southwest monsoon compared to pre-monsoon, and at southern locations along the west coast of India, it is 6–3% higher. In comparison to pre-monsoon, the mean wave period is 2-9% greater in post-monsoon (Fig. 9). Amrutha and Kumar (2017)

observed that in the nearshore waters of the eastern Arabian Sea, the H_{\max}/H_s ratio is 1.50-1.62 for different locations during the monsoon. In a year, the H_{\max} to H_s ratio in the eastern Arabian Sea varied from 1.3 to 2.6, with a mean value of 1.67 to 1.68 at different locations (Kumar and Mandal, 2020).

3.4 Distribution of wavelength

The wavelength corresponding to various wave periods estimated from half-hourly records from 2010 to 2019 are presented as a date versus year plot in Figure 8 and their statistical parameters are presented in Table 1. A similar pattern for $\lambda_{T1/3}$, λ_{Tc} , λ_{Ti} (Figs. 8f to 8h) is observed for the entire duration of the analysis. Most frequent values for λ_{Tp} occur within the wavelength of 90 m to 130 m. The average wavelength during June and July in different years varied from 61.3 m to 67.6 m, whereas the maximum wavelength varied from 216.6 m to 248.8 m. Interannual variations in average wavelength are up to 5.8%, while that of maximum wavelength is 8%. There is a large variation (24 to 115 m) in the maximum wavelength in a day due to the arrival of a few long-period waves. In various years, the maximum wavelength in each 30-minute record itself varied from 100 to 249 m. The variations in the 99-percentile wavelength in a day are comparatively low (14 to 81 m). The longest wave with a length of 248 m was in 2014.

The occurrence percent and the distribution of wavelength calculated from wave period using dispersion relation are shown in Figures 3b and 9. Half hourly mean values of wavelength based on the wave period from 2010 to 2019 at Ratnagiri are analysed in this section. Waves of longer wavelength (λ) travel faster than the shorter ones. In the Figure 3b, other than λ_{Tp} and λ_{Tc} , other parameters exhibit a similar shape. λ_{Tp} has a maximum occurrence of about 23.7% which is between 115 and 120 m. The values of wavelength corresponding to peak period (λ_{Tp}) ranges between 24.9 and 220.8 m (Fig. 9j) and the values for wavelength corresponding to mean wave period (λ_{Tm02}) goes up to a maximum value of 101.1 m and a minimum value of 21.3 m (Fig. 9b). In between 95 and 100 m, $\lambda_{T1/10}$ and λ_{Tdwl} has about 16.67% and 9.50% occurrence values. λ_{Tm01} and λ_{Ti} , have a maximum occurrence of 19.77% and 3.57% which occurs between 70-75 m and 100-105 m. Mean values of $\lambda_{T1/10}$ and λ_{Tm02} are 94.8 m and 59.7 m (Table 1). Variation of λ_{Tdwl} (Fig. 9k) is between 28 m and 211.8 m and $\lambda_{Tm-1,1}$ varies between 35.8 m and 119 m. There is about zero number of values for λ_{Tm01} , $\lambda_{Ti} > 125$ m. Wavelength corresponding to the integral period (λ_{Ti}) varies between 56.7 m to 133.5 m (Fig. 9f). 75-percentile values of λ_{Tc} show a value of 26.4 m and indicate that most values of λ_{Tc} are less than 26.4 m. Along Ratnagiri, 47.47% of λ_{Tc} lies in between 20-25 m and 21.74% of λ_{Tavg} lies in between 60-65 m. λ_{Tavg} (Fig. 9d) and λ_{THmax} (Fig. 9i) varies between 24.9 to 111.5 m and 21.3 to 176.8 m. Mode values for λ_{Ti} , λ_{Tpc} , $\lambda_{Tm-1,1}$ are 91.7 m, 123.5 m and 78.9 m. The individual

wavelength of waves based on their corresponding wave period shows a range of 244.2 m. The 25-percentile values of λ_{Tm01} and T_e are up to 63.7 and 79.6 m.

3.5 Interannual variations in wavelength corresponding to various wave periods

The interannual variations in wavelength from 2010 to 2019 are presented in Fig 6d to 6f. The wavelength corresponding to the peak period (λ_{Tp}) is mostly concentrated in a range of 24.9–220.8 m and their 99-percentile value has the highest variation over the years (Fig. 6d) and the lowest variation is seen for the parameter λ_{Tc} . The mean value of all wavelengths are lowest in 2015 (Fig. 6f) and the 99-percentile values of λ_{Tp} were highest during 2014 and 2016.

The interannual variations in the 90-percentile values for wavelength (λ) are up to 5% and show a positive and negative variation across the years. Similar changes are observed for wave period (T) where the year-to-year variation in 90-percentile values is up to 4%. The 90-percentile and the mean value of λ_{Tc} reached a maximum of 31 m and 24.7 m, respectively in 2010 and the mean value was lowest (21.6 m) in 2015. Interannual variations in the 90-percentile value of λ_{Tp} is up to 16% (Fig. 6e). The 90-percentile and mean values of wavelengths and wave periods, as well as the observed interannual fluctuations in these values, demonstrate the dynamic character of oceanic patterns. The variation in the mean value of λ_{Tc} is less than 5% (Fig. 6f). A maximum 99-percentile value for λ_{Tm02} , λ_{Tm01} , λ_{Tavg} , λ_{Tdw1} of about 90.9 m, 104.4 m, 98.1 m and 174.2 m are observed in 2014. The values of λ_{Te} vary between 45.3 m and 127.7 m with a maximum mean value of 88.3 m in 2010 and the 90-percentile value (91.7 m) is lower for 2011. Mean values of λ_{Tp} and λ_{Ti} are the maximum for 2014 (122 m and 95.2 m), the higher values are the result of an extreme event (Tropical Cyclone Nanauk) that occurred in the Arabian Sea during June. The variation of all parameters for the year 2019 is less than 2%. Except in 2014, fewer variations were observed in wavelength. The studies related to wavelength based on various wave periods are useful for designing marine infrastructure. Interannual variations in the 90-percentile values for $\lambda_{T1/3}$ and λ_{THmax} are up to 6% and 7% respectively.

4. Conclusions

The wave period measured at 13 m depth off Ratnagiri in the coastal waters of the eastern Arabian Sea from 2010 to 2019 indicates that most frequent waves are within a wave period of 3.9 s to 5.5 s. The water depth at the buoy location is considered constant (13 m), which is not the case since there will be a change in water depth due to tide with an average tidal range of 2.1 m and it will result in a change in the wavelength presented in this article. During monsoon months June and July, about 50% of all seas are within the period range of 4.7–9.0 s. The distribution of wave periods at the

study region shows that among all the years analysed the wave periods during 2014 exceeded more than the other wave periods except in the case of T_p and T_c . The date versus year plot shows a similar pattern for $T_{1/3}$, T_i , and T_c . At Ratnagiri, long-period waves ($T_p > 8s$) dominate with a percentage of 98.45. In June and July from 2010 to 2019, the distribution of wave period of individual waves reveals that considerably longer waves ($T > 12 s$) are more prevalent in 2014, while shorter waves ($T < 4 s$) are more prevalent in 2015. The influence of Tropical cyclone Nanauk on wave period and on annual variations are discussed. The 99-percentile values for T_{m02} and T_{m01} show up to 10% and 11% interannual variance. Interannual changes in the 90-percentile of T_p is up to 15% and λ_{Tp} is up to 16%. The relationship of wave periods is studied and the result shows a strong linear relationship for T_c with T_i and $T_{1/3}$ and implies that changes in T_i and $T_{1/3}$ have an effect on the energy wave period. The maximum wavelength varied from 216.6 m to 248.8 m during June and July. Up to 5.8% of the average wavelength varies annually. The mean value for λ_{Tc} was lowest (21.6 m) in 2015. Interannual variations in the 90-percentile values for $\lambda_{T1/3}$ and λ_{THmax} are up to 7% and 5%. This study emphasizes how wave parameters, such as wave period and wavelength, vary from year to year. It provides information on the dynamic nature of wave patterns in this area by quantifying these variations. The results presented here can be used for selecting a suitable wave energy convertor for the study area. For many applications, including coastal engineering and navigation, understanding interannual variability in wave period and wavelength is essential. The wavelength changes with water depth and hence, the values presented in the study are for a particular water depth. The impact of various atmospheric oscillations such as El Niño Southern Oscillation (ENSO), Southern Annular Mode (SAM), Indian Ocean Dipole (IOD) and Boreal Summer Intra-Seasonal Oscillation (BSISO) on the wave period and wavelength are not examined in the present study.

Conflict of interests

The authors declare that they have no known competing financial interests or personal relationships that could have appeared to influence the work reported in this paper.

Data availability

The data used in this study is available at INCOIS (http://www.incois.gov.in/Incois/info_insitu.jsp)

Credit authorship contribution statement

Anju: Conceptualization; Data curation; Formal analysis; Investigation; Methodology; Visualization; Writing - original draft

Sanil Kumar: Conceptualization; Resources; Supervision; Writing - review & editing.

Jai Singh: Data curation

Bhaware B.G: Data curation

Declaration

We have not used any copyright material in this paper. The authors declare that they have no known competing financial interests or personal relationships that could have appeared to influence the work reported in this paper.

Acknowledgments

The authors gratefully acknowledge the financial support given by the Council of Scientific & Industrial Research, New Delhi to conduct this research. The wave data used in the study are from the project funded by Earth System Science Organization, Ministry of Earth Sciences, Government of India through INCOIS, Hyderabad. The authors thank both the reviewers for the comments and suggestions, which improved the content of the paper. This is NIO contribution ---.

References

- Ahn, S., 2021. Modeling mean relation between peak period and energy period of ocean surface wave systems. *Ocean Engineering*, 228, Article number 108937.
- Amrutha, M.M., Kumar, V.S., 2017. Characteristics of high monsoon wind-waves observed at multiple stations in the eastern Arabian Sea, *Ocean Science Discussions*, <https://doi.org/10.5194/os-2017-84>.
- Anjali Nair, M., Amrutha, M.M., Kumar, V.S., 2022. Spectral wave characteristics in the coastal waters of the central west coast of India during tropical cyclone Kyarr, *Ocean Dynamics*, 72:151–168, <https://doi.org/10.1007/s10236-022-01496-x>
- Anjali Nair, M., Kumar, V.S., Amrutha, M.M., 2018. Spectral Wave Characteristics in the Nearshore Waters of Northwestern Bay of Bengal. *Pure Appl. Geophys.* 175, 3111–3136, <https://doi.org/10.1007/s00024-018-1838-5>
- Anju, T. M., Kumar, V.S., 2023. Steepness of surface gravity waves measured in the eastern Arabian Sea during peak monsoon months, *Ocean Engineering* 280, Article number 114900. <https://doi.org/10.1016/j.oceaneng.2023.114900>
- Anoop, T.R., Kumar, V.S., Shanas, P.R., Johnson, G., 2015. Surface wave climatology and its variability in the North Indian Ocean based on ERA-Interim reanalysis, *Journal of Atmospheric and Oceanic Technology* 32,7, 1372-1385, doi.: 10.1175/JTECH-D-14-00212.1
- Anoop, T.R., Kumar, V.S., Shanas, P.R., Johnson, G., Amrutha, M.M., 2016. Indian Ocean Dipole modulated wave climate of eastern Arabian Sea, *Ocean Science*, 12, 369-378, <https://doi.org/10.5194/os-12-369-2016>

- Anusree, A., Kumar, V.S., 2023. Variations in short-term statistics of waves observed in the coastal waters of the eastern Arabian Sea, *Ocean Engineering* 281, Article number 114824. <https://doi.org/10.1016/j.oceaneng.2023.114824>
- Bradbury, A. P., Mason, T. E., Poate, T., 2007. Implications of the spectral shape of wave conditions for engineering design and coastal hazard assessment - Evidence from the English Channel, in 10th International workshop on wave hindcasting and forecasting and coastal hazard symposium, 5 pp. 1–17.
- Bromirski, P.D., Cayan, D.R., Flick, R.E., 2005. Wave spectral energy variability in the northeast Pacific. *Journal of Geophysical Research*, 110(C3). <https://doi.org/10.1029/2004JC002398>.
- Chun, H., Ahn, K., 2017. Storm waves on the East coast of Korea: 20 years of wave hindcasting. *Journal of Coastal Research*, 33(5), 1182-1188.
- Chun, H., Suh, K. D., 2018. Estimation of significant wave period from wave spectrum. *Ocean Engineering*, 163, 609-616.
- Contestabile, P., Ferrante, V., Vicinanza, D., 2015. Wave Energy Resource along the coast of Santa Catarina (Brazil). *Energies* 8, 14219–14243. doi:10.3390/en81212423.
- Datawell, 2009. *Datawell Waverider Reference Manual*, Datawell BV oceanographic instruments, The Netherlands, pp 123.
- George, J., Kumar, V.S., 2020. Climatology of wave period in the Arabian Sea and its variability during the recent 40 years, *Ocean Engineering* 216, Article number 108014, doi.org/10.1016/j.oceaneng.2020.108014.
- George, J., Kumar, V.S., 2021. Spectral peak wave period climatology and its relationship with natural climate variability over the Bay of Bengal, *Ocean Dynamics*, 71, 871–892, <https://doi.org/10.1007/s10236-021-01473-w>
- Glejin, J., Kumar, V. S., Singh, J., 2015. Inter-annual variations in wave characteristics off Ratnagiri, Northeast Arabian Sea. *Aquatic procedia*, 4, 25-31.
- Goda, Y., 2010. *Random Seas and Design of Maritime Structures*. World Scientific Inc., Singapore.
- Günther, H., Hasselmann, S., Janssen, P.A.E.M., 1992. WAM model Cycle 4 (Revised Version). Deutsches Klimarechenzentrum Technical Report No. 4.
- Hemer, M. A., Zieger, S., Durrant, T., O’Grady, J., Hoeke, R. K., McInnes, K. L., Rosebrock, U., 2017. A revised assessment of Australia's national wave energy resource. *Renewable Energy*, 114, 85–107. <https://doi.org/10.1016/j.renene.2016.08.039>
- Hemer, M. A., Church, J. A., Hunter, J. R. 2010. Variability and trends in the directional wave climate of the Southern Hemisphere. *International Journal of Climatology*, 30(4), 475-491. <https://doi.org/10.1002/joc.1900>
- Hofland, B., Chen, X., Altomare, C., Oosterlo, P., 2017. Prediction formula for the spectral wave period $T_{m-1,0}$ on mildly sloping shallow foreshores. *Coastal Engineering*, 123, 21-28.

India Meteorological Department, 2014. Cyclonic Storm, 'NANAUK' over the Arabian Sea (10-14 June 2014): A Report. Cyclone Warning Division, New Delhi, India

Joseph, D., Kumar, V.S., 2021. Response of ocean surface waves to the co-occurrence of Boreal Summer Intra-Seasonal Oscillation and El Niño Southern Oscillation. *Climate Dynamics*, 57, 1155–1171, <https://doi.org/10.1007/s00382-021-05763-3>

Kumar V.S., George, J., Joseph, D., 2020. Hourly maximum individual wave height in the Indian shelf seas - its spatial and temporal variations in recent 40 years, *Ocean Dynamics* 70:1283–1302, [10.1007/s10236-020-01395-z](https://doi.org/10.1007/s10236-020-01395-z)

Kumar, P., Kaur, S., Weller, E., Min, S.K., 2019. Influence of natural climate variability on the extreme ocean surface wave heights over the Indian Ocean. *Journal of Geophysical Research: Oceans*, 124. <https://doi.org/10.1029/2019JC015391>

Kumar, V.S., George, J., 2016. Influence of Indian summer monsoon variability on the surface waves in the coastal regions of eastern Arabian Sea, *Annales Geophysicae*, 34, 871–885, 2016. <https://doi.org/10.5194/angeo-34-871-2016>

Kumar, V.S., Kumar, K.A., Anand, N.M., 2000. Characteristics of waves off Goa, West coast of India, *Journal of Coastal Research*, 16(3), 782-789, www.jstor.org/stable/4300088

Kumar, V.S., Mandal, S., 2022, Characteristics of individual surface waves measured by moored buoys in the coastal waters of the eastern Arabian Sea, *Ocean Engineering*, 248, Article number 110861, doi.org/10.1016/j.oceaneng.2022.110861.

Kumar, V.S., Shanas, P.R, Dubhashi, K.K, 2014, Shallow water wave spectral characteristics along the eastern Arabian Sea, *Natural Hazards* 70, 377–394, DOI [10.1007/s11069-013-0815-7](https://doi.org/10.1007/s11069-013-0815-7)

Liu, J., Meucci, A., Liu, Q., Babanin, A. V., Ierodiaconou, D., Young, I. R., 2022. The wave climate of Bass Strait and south-east Australia. *Ocean Modelling*, 172, 101980. <https://doi.org/10.1016/j.ocemod.2022.101980>.

Liu, J., Meucci, A., Young, I. R., 2023. A comparison of multiple approaches to study the modulation of ocean waves due to climate variability. *Journal of Geophysical Research: Oceans*, 128, e2023JC019843. <https://doi.org/10.1029/2023JC019843>.

Mendes, D., Oliveira, T. C., 2021. Deep-water spectral wave steepness offshore mainland Portugal. *Ocean Engineering*, 236, 109548.

Rao, C.V.K.P., Baba, M., 1996. Observed wave characteristics during growth and decay: a case study. *Cont Shelf Res.* 16(12), 1509–1520.

Rawat, A., Ardhuin, F., Ballu, V., Crawford, W., Corela, C., and Aucan, J., 2014. Infragravity waves across the oceans, *Geophys. Res. Lett.*, 41, 7957–7963, doi:[10.1002/2014GL061604](https://doi.org/10.1002/2014GL061604).

Shen, W.J., Gao, F., Chen, Q., Mao, C.L., 2016. Study the effect of long-period waves on mooring large vessel, In: *Advances in Engineering Materials and Applied Mechanics – Zhang, Gao and Xu (Eds) Taylor & Francis Group, London, ISBN 978-1-138-02834-0*

Stokes, G.G., 1880. Considerations Relative to the Greatest Height of Oscillatory Irrotational Waves Which Can Be Propagated without Change of Form. In *On the Theory of Oscillatory Waves*; Cambridge University Press: London, UK, 225–229.

Suzuki, H., Yoshida, K., Iijima K., 1996. A consideration of the structural design of a largescale floating structure. *Journal of Marine Science and Technology*, 1(5), 255–267.

Tucker, M.J., 1991. *Waves in ocean engineering: measurement, analysis, interpretation*. Ellis Horwood, Chichester, UK. 431 pp.

Ueda, S., 2015. Floating Oil Storage Base. In: Wang, C., Wang, B. (eds) *Large Floating Structures. Ocean Engineering & Oceanography*, vol 3. Springer, Singapore. https://doi.org/10.1007/978-981-287-137-4_4

Van der Meer, J. W., Allsop, N. W. H., Bruce, T., De Rouck, J., Kortenhaus, A., Pullen, T., Schüttrumpf, H., Troch, P., Zanuttigh, B., 2016. *EurOtop 2016: Manual on wave overtopping of sea defences and related structures. An overtopping manual largely based on European research, but for worldwide application., Second Edi., 2016.*

WMO, 1998. *Guide to Wave Analysis and Forecasting*, WMO No.-702, World Meteorological Organization – Geneva – Switzerland.

Young, I. R., 1999. Seasonal variability of the global ocean wind and wave climate. *International Journal of Climatology*, 19(9), 931–950. [https://doi.org/10.1002/\(sici\)1097-0088\(199907\)19:9<931:AID-JOC412>3.0.CO;2-O](https://doi.org/10.1002/(sici)1097-0088(199907)19:9<931:AID-JOC412>3.0.CO;2-O)

Annexure. Notations and definition of wave parameters used in the study

d = water depth at the measurement location

H_s = significant wave height = $4\sqrt{m_0}$

T = individual wave period

T_{avg} = average wave period in a record of 30-min

$T_e = T_{m-1,0}$ = wave energy period = $\frac{m_{-1}}{m_0}$

T_{m02} = mean zero-crossing wave period = $\sqrt{\frac{m_0}{m_2}}$

$T_{m-1,1}$ = average wave period = $\sqrt{\frac{m_{-1}}{m_1}}$

T_i = integral period = $\sqrt{\frac{m_{-2}}{m_0}}$

T_{m01} = mean period = reciprocal number of mean frequency of wave spectrum = m_0/m_1

T_c = crest period = mean time interval for the local maxima = $\sqrt{m_2/m_4}$

T_{dw1} = $\sqrt{m[-1,2] / m_0}$

T_{pc} = calculated peak period = $m_{-2} m_1/m_0^2$

T_p = peak wave period = inverse of the wave frequency at the spectral peak

T_{Hmax} = period of the highest wave

$T_{1/10}$ = average period of 10% highest waves

$T_{1/3}$ = significant wave period = average period of 33% highest waves

where m_n is the nth order spectral moment $m_n = \int_0^{\infty} f^n S(f) df$, $n=0, 1, 2, -1$, and $S(f)$ is spectral energy density at frequency f .

λ = wavelength at the measurement location of wave estimated as per dispersion relationship from period

λ_X = wavelength estimated from wave period X

Table 1. Statistical parameters of different wave periods and corresponding wavelengths for data covering June and July from 2010 to 2019

Parameter	Minimum	Maximum	Range	Mean	Mode	First quartile (25-percentile)	Third quartile (75-percentile)
Wave period (s)							
T_c	2.4	5.8	3.4	3.9	3.8	3.7	4.1
T_{m02}	3.7	9.9	6.2	6.6	6.8	6.2	7.1
T_{avg}	4.0	10.7	6.7	6.9	7.0	6.4	7.4
T	1.6	21.6	20.0	6.9	3.9, 5.5	4.7	9.0
T_{m01}	4.2	10.7	6.5	7.4	7.8	6.9	7.9
$T_{m-1,1}$	4.8	11.3	6.5	8.1	8.1	7.5	8.6
T_e	5.5	12.0	6.5	8.7	9.0	8.1	9.2
$T_{1/3}$	4.9	12.8	7.9	9.1	9.5	8.4	9.7
T_i	6.4	12.5	6.2	9.2	9.1	8.7	9.8
T_{Hmax}	3.7	16.2	12.5	9.3	9.6	8.4	10.3
$T_{1/10}$	5.4	12.7	7.3	9.3	9.4	8.7	10.0
T_{dwl}	4.3	19.2	15.0	9.8	9.8	8.7	10.9
T_p	4.0	20.0	16.0	11.1	11.1	10.5	11.8
T_{pc}	8.7	19.1	10.4	11.5	11.7	10.9	12.2
Wavelength corresponding to wave period (m)							
λ_{Tc}	8.8	49.0	40.2	23.6	22.5	20.9	26.4
λ_{Tm02}	21.3	101.1	79.8	59.7	61.7	53.6	65.9
λ_{Tavg}	24.9	111.5	86.6	63.5	65.0	57.0	70.2
λ_T	4.0	248.2	244.2	65.0	12.8	33.6	93.7
λ_{Tm01}	27.0	111.5	84.5	70.4	75.1	63.7	77.1
$\lambda_{Tm-1,1}$	35.8	119.0	83.2	78.5	78.9	71.8	85.2
λ_{Te}	45.3	127.7	82.4	86.7	88.9	79.6	93.6
$\lambda_{T1/3}$	36.6	136.8	100.2	91.1	96.8	83.1	99.3
λ_{Ti}	56.7	133.5	76.8	93.6	91.7	86.8	100.2
λ_{THmax}	21.3	176.8	155.5	94.6	98.1	83.1	106.7
$\lambda_{T1/10}$	43.4	135.6	92.2	94.8	95.6	86.8	103.0
λ_{Tdwl}	28.0	211.8	183.8	100.7	101.0	86.2	114.0
λ_{Tp}	24.9	220.8	195.9	116.1	116.5	109.5	124.3
λ_{Tpc}	86.7	210.7	124.0	121.7	123.5	113.4	129.1

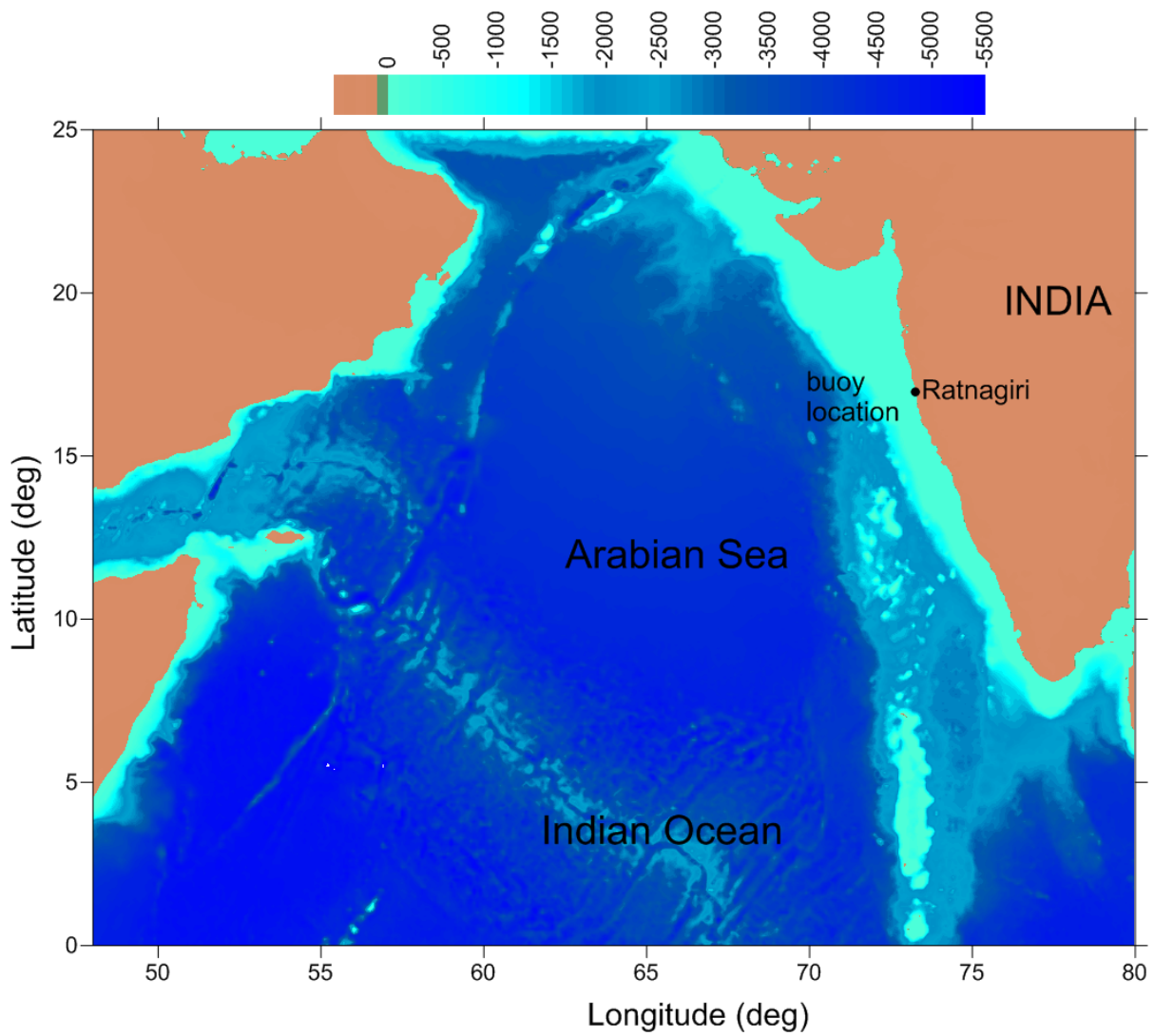


Figure 1. Map showing the location of waverider buoy location in the eastern Arabian Sea. The colour shade is the water depth in metre

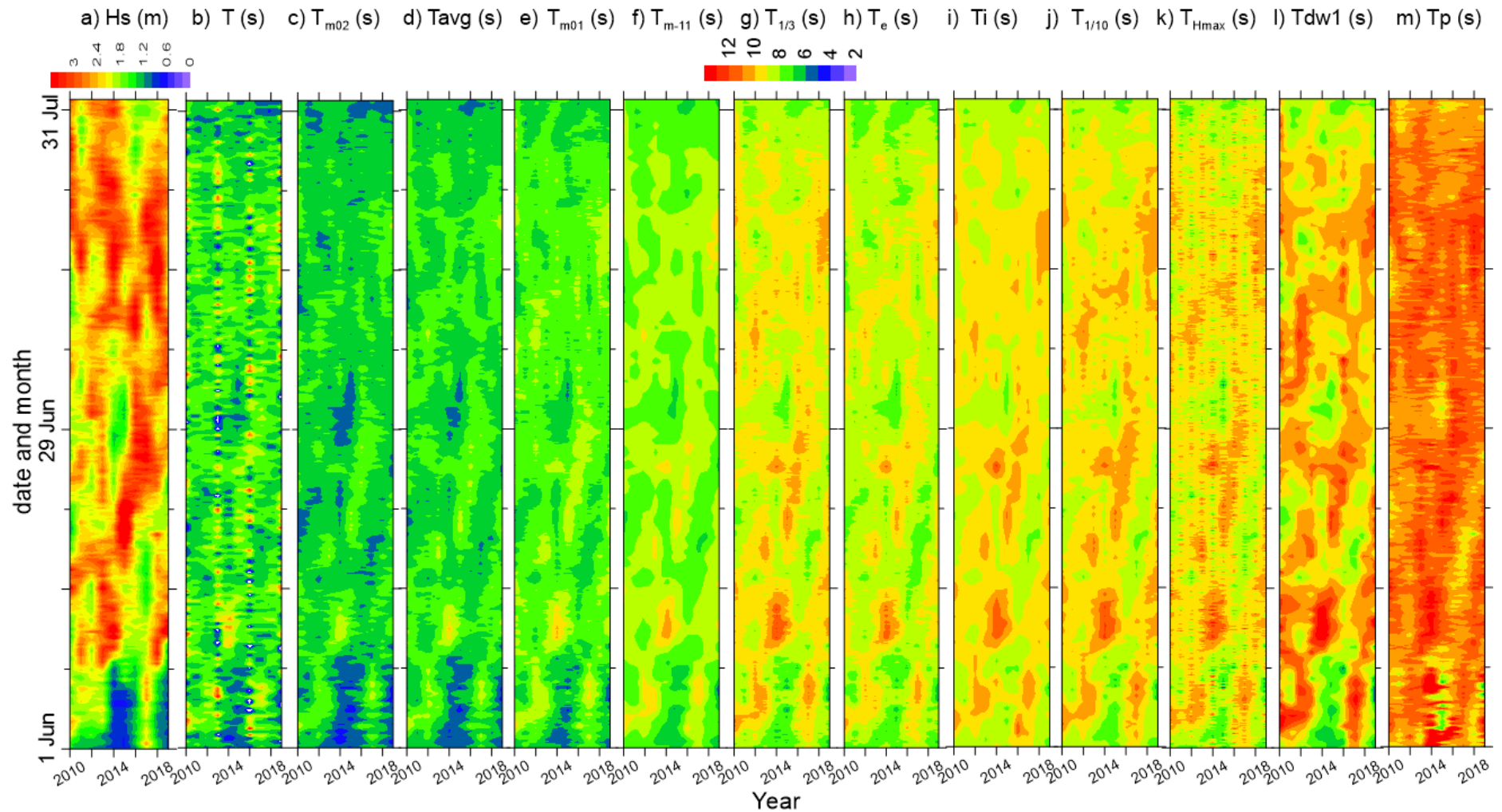


Figure 2. Date versus year plots of a) significant wave height, b) period of individual waves, c) mean zero-crossing period, d) average wave period, e) mean period, f) average period, g) average period of 33% highest waves, h) energy period, i) integral period, j) average period of 10% highest waves, k) period of the highest wave, l) T_{dw1} , m) peak wave period

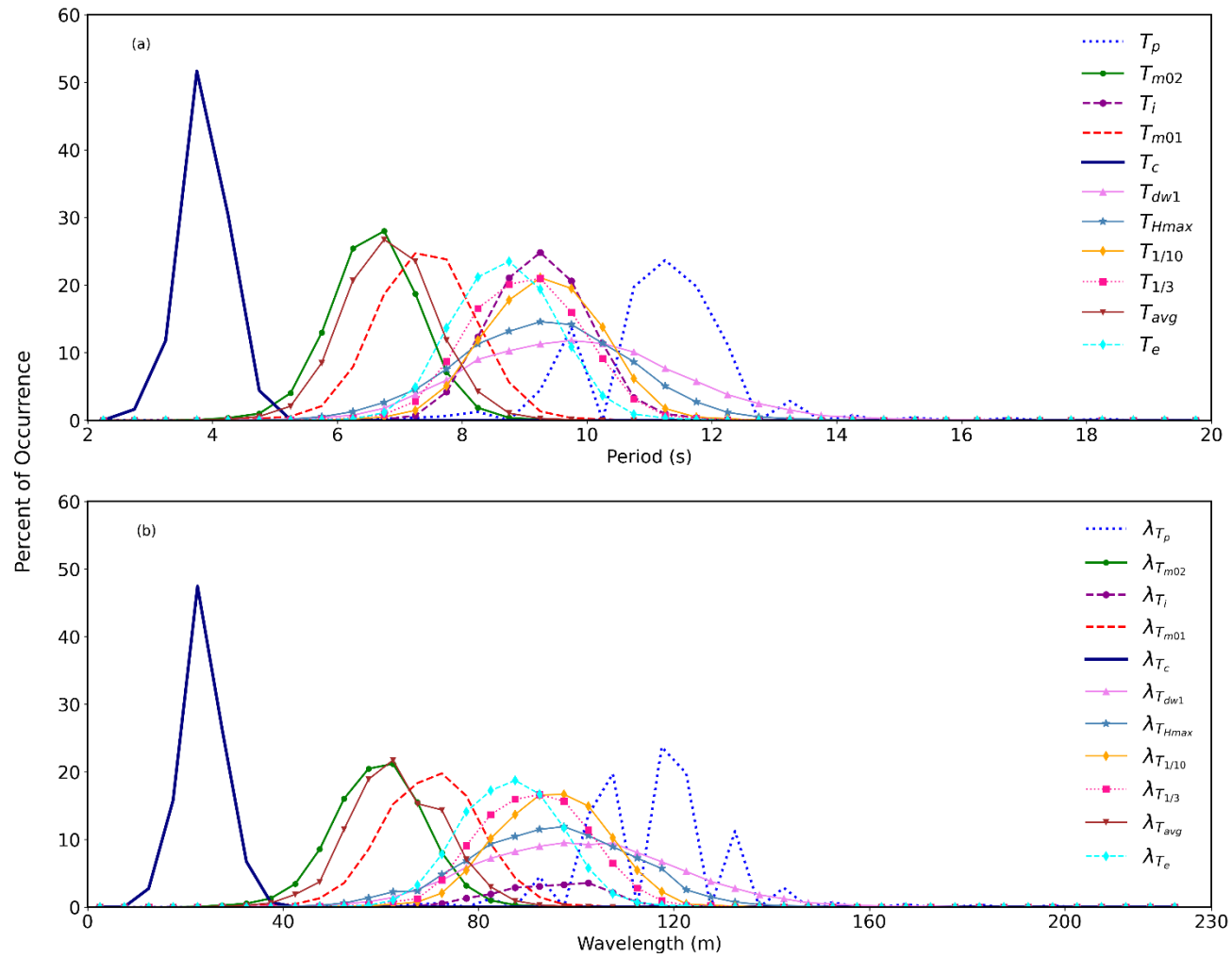


Figure 3. Percentage occurrence of different wave periods (a) and its corresponding wavelength (b) at Ratnagiri from 2010 to 2019 during peak monsoon months

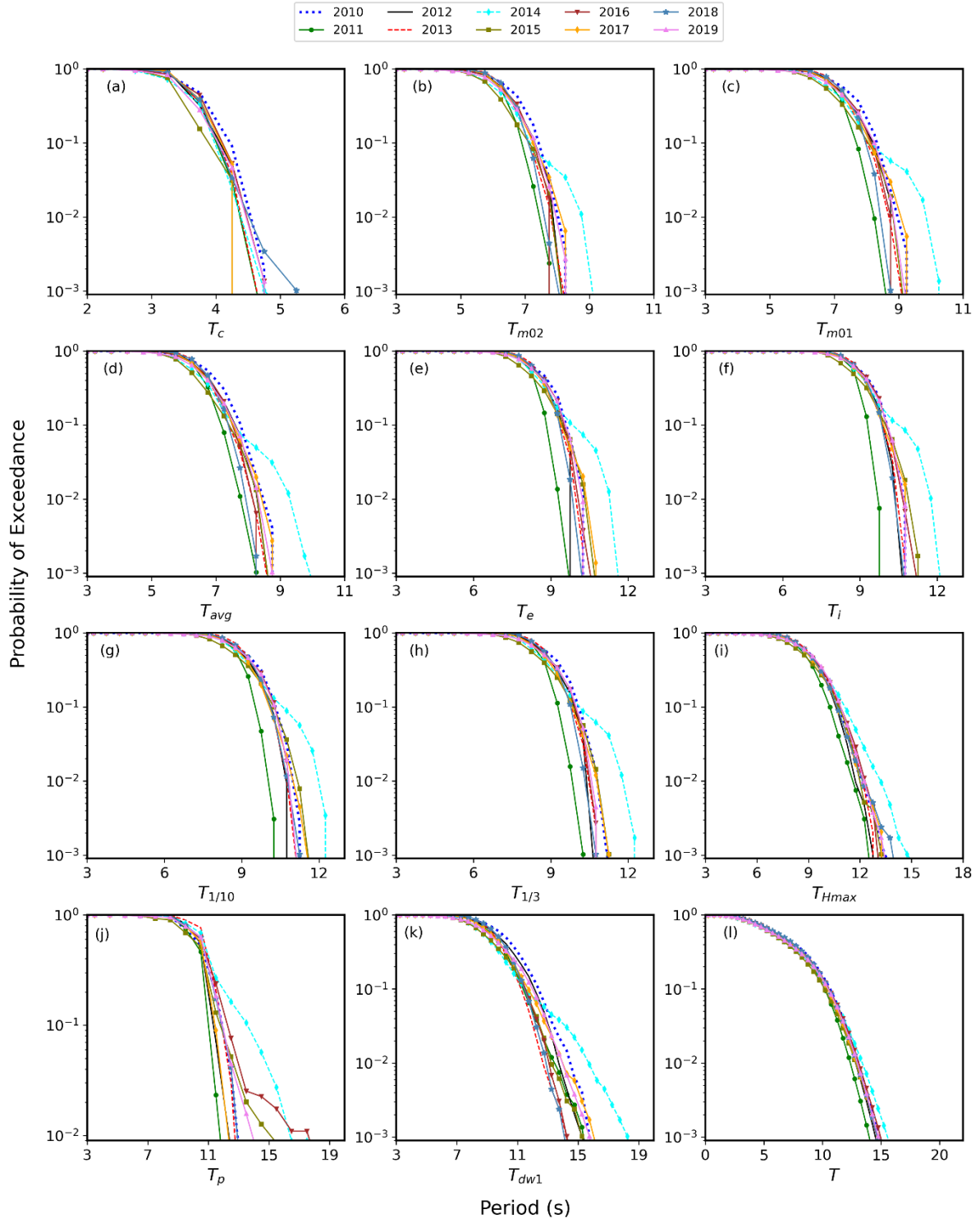


Figure 4. Distribution of various wave periods at Ratnagiri from 2010 to 2019 during the peak monsoon months

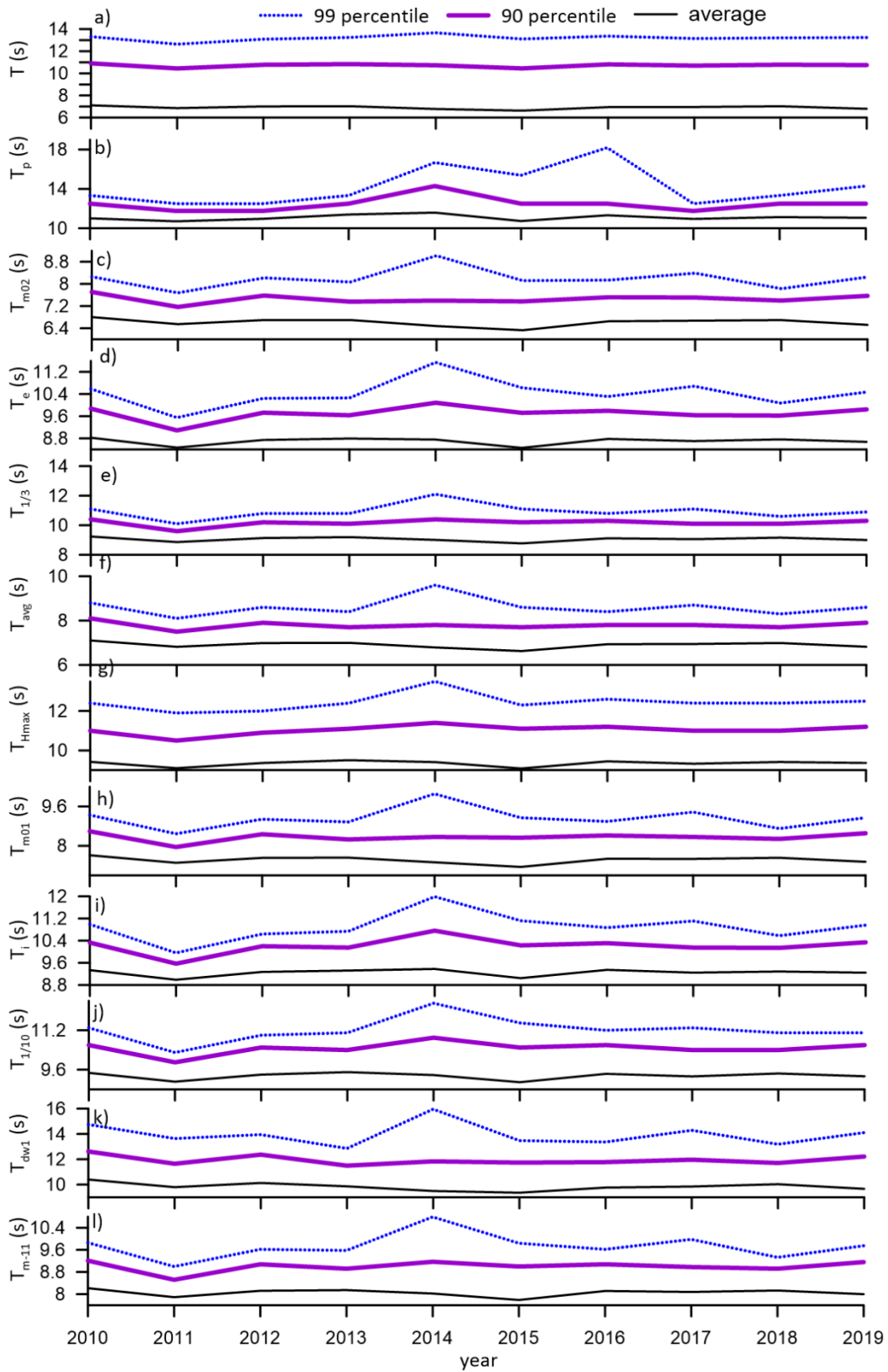


Figure 5. 99-percentile, 90-percentile and average value of a) wave period of individual wave, b) peak wave period, c) mean zero-crossing wave period, d) energy period, e) average period of 33% highest waves, f) average period in 30-min record, g) period of the maximum wave height, h) mean period i) integral period, j) average period of 10% highest waves, k) T_{dwl} and l) average period in June and July of different years

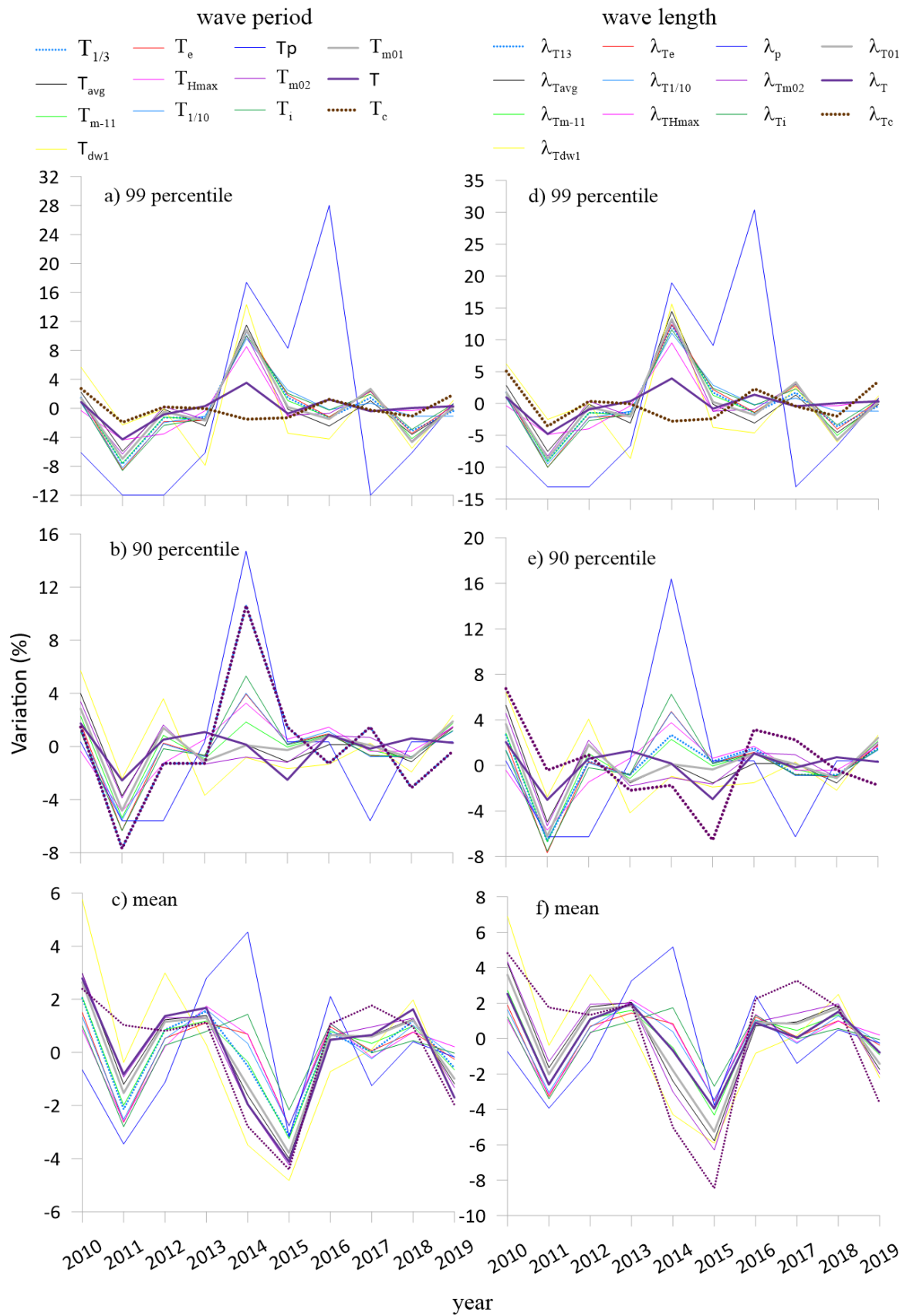


Figure 6. Interannual variations in 99-percentile, 90-percentile and mean values of different wave periods (a to c) and corresponding variations in wavelength (d to f)

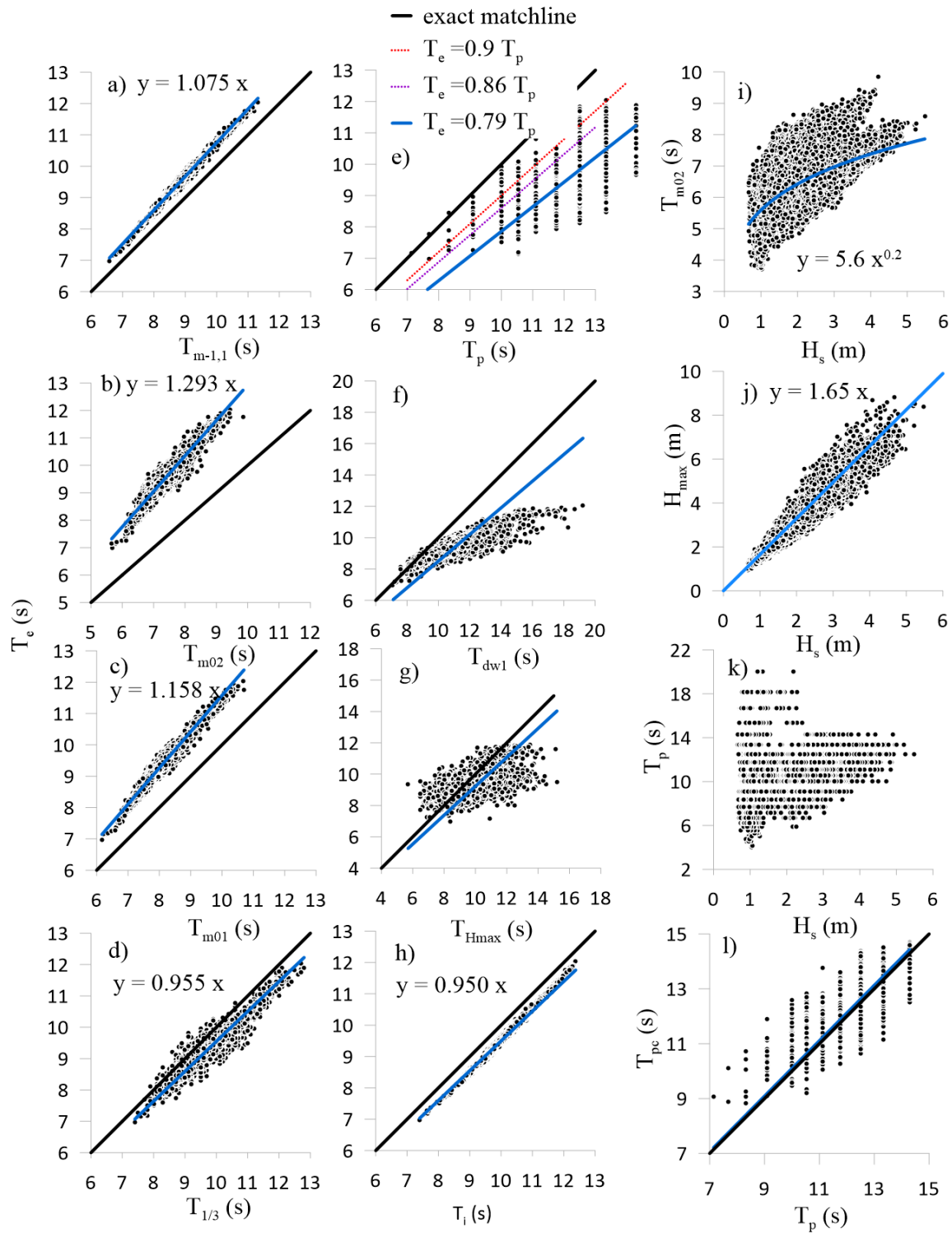


Figure 7. Inter comparison of T_e with various wave periods a) $T_{m-1,1}$, b) T_{m02} , c) T_{m01} , d) $T_{1/3}$, e) T_p , f) T_{dwl} , g) T_{Hmax} , h) T_i . Scatter plots of H_s with i) T_{m02} , j) H_{max} and k) T_p . l) scatter plot of T_p with T_{pc}

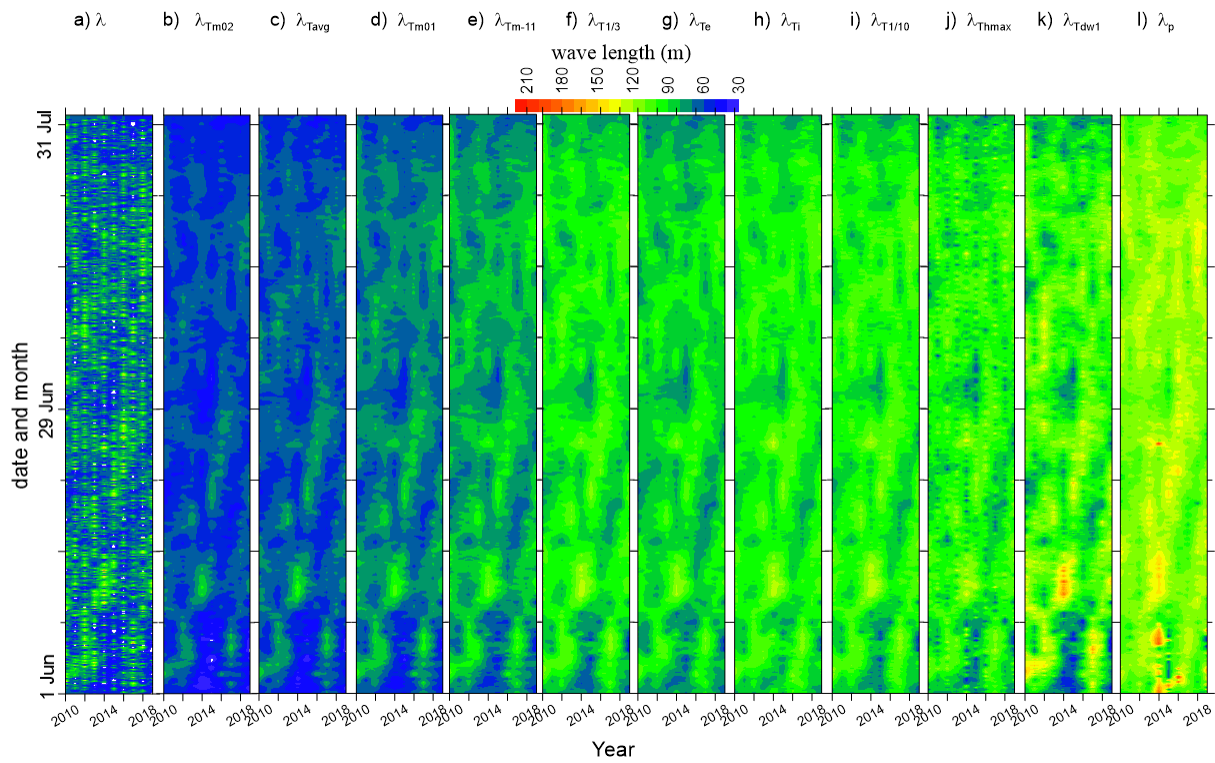


Figure 8. Temporal distribution of wavelengths corresponding to various wave periods a) period of individual wave, b) mean zero-crossing period, c) average wave period, d) mean period, e) average period, f) average period of 33% highest waves, g) energy period, h) integral period, i) average period of 10% highest waves, j) period of the highest wave, k) Tdw1, l) peak wave period

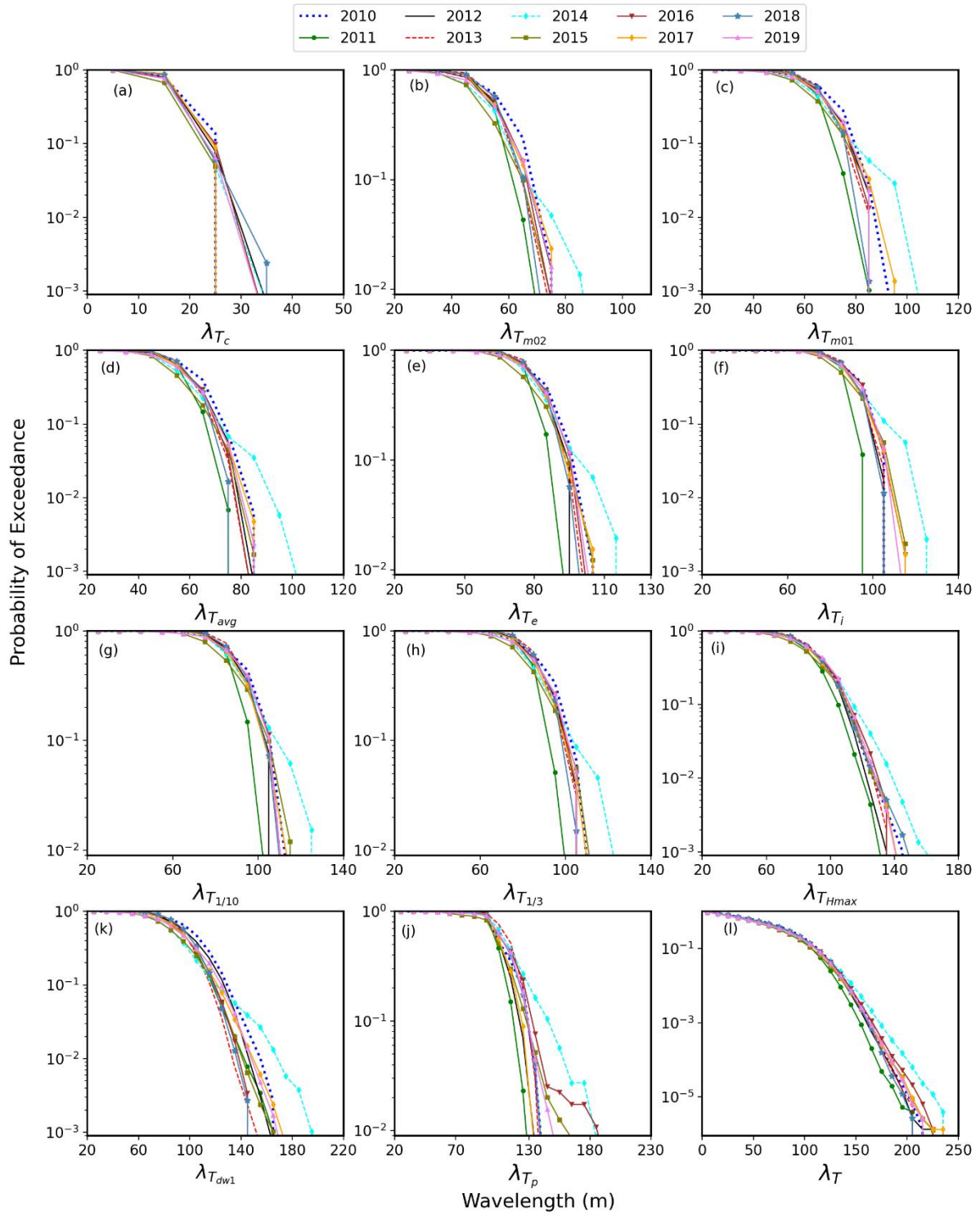


Figure 9. Distribution of wavelength corresponding to different wave periods at Ratnagiri from 2010 to 2019 during the peak monsoon months